Earth **Surface**
Dynamics
Discussions

Open Access

Analysis of glacial and periglacial processes using structure from motion

L. Piermattei[1], **L. Carturan**[1], **F. de Blasi**[1], **P. Tarolli**[1], **G. Dalla Fontana**[1], **A. Vettore**[2], and **N. Pfeifer**[3]

[1]Department of Land, Environment, Agriculture and Forestry, University of Padova, Italy
[2]Interdepartment Research Center of Geomatics, University of Padova, Italy
[3]Department of Geodesy and Geoinformation, TU Wien, Austria

Correspondence to: L. Piermattei (livia.piermattei@studenti.unipd.it)

Discussion Paper | Discussion Paper | Discussion Paper | Discussion Paper

ESURFD

3, 1345–1398, 2015

Analysis of glacial and periglacial processes using SfM

L. Piermattei et al.

Title Page

Abstract	Introduction
Conclusions	References
Tables	Figures

|◀ ▶|

◀ ▶

Back Close

Full Screen / Esc

Printer-friendly Version

Interactive Discussion

Analysis of glacial and periglacial processes using SfM

L. Piermattei et al.

Abstract

Close-range photo-based surface reconstruction from the ground is rapidly emerging as an alternative to lidar (light detection and ranging), which today represents the main survey technique in many fields of geoscience. The recent evolution of photogramme-
try, incorporating computer vision algorithms such as Structure from Motion (SfM) and dense image matching such as Multi-View Stereo (MVS), allows the reconstruction of dense 3-D point clouds for the photographed object from a sequence of overlapping images taken with a digital consumer camera. The objective of our work was to test the accuracy of the ground-based SfM-MVS approach in calculating the geode-
tic mass balance of a $2.1\,\mathrm{km}^2$ glacier in the Ortles-Cevedale Group, Eastern Italian Alps. In addition, we investigated the feasibility of using the image-based approach for the detection of the surface displacement rate of a neighbouring active rock glacier. Airborne laser scanning (ALS) data were used as benchmarks to estimate the accu-
racy of the photogrammetric DTMs and the reliability of the method in this specific application. The glacial and periglacial analyses were performed using both range and image-based surveying techniques, and the results were then compared. The results were encouraging because the SfM-MVS approach enables the reconstruction of high-quality DTMs which provided estimates of glacial and periglacial processes similar to those achievable by ALS. Different resolutions and accuracies were obtained for the glacier and the rock glacier, given the different survey geometries, surface characteris-
tics and areal extents. The analysis of the SfM-MVS DTM quality allowed us to highlight the limitations of the adopted expeditious method in the studied alpine terrain and the potential of this method in the multitemporal study of glacial and periglacial areas.

1 Introduction

Knowledge of changes in the extent, mass and surface velocity of glaciers and rock glaciers contributes to better understanding the dynamic processes occurring in cold

high-mountain environments and serves as an important contribution to climate monitoring (Kääb et al., 2003).

Numerous techniques exist for monitoring and quantifying these changes and include both field and remote sensing methods (Immerzeel et al., 2014). Fieldwork generally yields high-quality data but with a small spatial extent, given the remoteness and low accessibility of mountain areas at high elevations (Roer et al., 2007). Therefore, using remotely sensed datasets for at least two different points in time has become an important tool for monitoring high-mountain terrain dynamics (Kääb, 2002). Multi-temporal Digital Terrain Models (DTMs) based on remote sensing data are the most commonly used products for such investigations (Kääb, 2005; Tseng et al., 2015).

Among the many remote sensing techniques, aerial photogrammetry is the oldest method, and it has a long history of application in the study of glaciers (Welch and Howarth, 1968; Kääb and Funk, 1999; Schenk, 1999; Baltsavias et al., 2001; Kääb 2005; Haug et al., 2009; Bühler et al., 2014; Müller et al., 2014) and the monitoring of rock glaciers via repeated stereo images (Kääb et al., 1997; Kaufmann, 1998; Kääb, 2003; Fischer, 2011). Terrestrial (ground-based or close-range) photogrammetry was one of the first measurement techniques used to map high mountain terrain and for reliably measuring the flow velocity of a rock glacier (Kaufmann and Ladstädter 2007; Kaufmann, 2012) until it was replaced by aerial and spaceborne platforms (Pellikka and Rees, 2009).

Over the last decade, the photogrammetric technique has widely been replaced by lidar (light detection and ranging) technology, which has progressively become the primary survey technique in geomorphology (Tarolli, 2014). Aerial laser scanning (ALS) is reported to be a very accurate method for DTM generation in alpine terrain (Bülher and Graf, 2013; Aguilar and Mills, 2008; Höfle and Rutzinger, 2011), snow covered areas (Höfle et al., 2007; Deems et al., 2013) and glacial environments (Geist Stotter, 2007; Kodde et al., 2007; Abermann et al., 2010; Knoll and Kerschner, 2010; Carturan et al., 2013; Colucci et al., 2014; Joerg and Zemp, 2014). However, aerial lidar surveys are

Analysis of glacial and periglacial processes using SfM

L. Piermattei et al.

still expensive and terrestrial lidar surveys involve expensive and logistically demanding equipment.

The recent evolution of digital photogrammetry, based on computer vision algorithms, has led to a rapid revival of close-range photogrammetry as the major alternative to traditional surveying techniques and lidar, due to its lower cost, high portability, and easy and rapid surveying in the field.

The photogrammetric approach known as Structure from Motion (SfM) obtains 3-D information on the photographed object from a sequence of overlapping images taken with a common digital camera. The ability to obtain 3-D models with accuracies and resolutions comparable to those of lidar has created new opportunities, especially in geoscience applications in remote areas (James and Robson, 2012; Bemis et al., 2014; Micheletti et al., 2014; Prosdocimi et al., 2015; Stumpf et al., 2015). An overview of the SfM applications and accuracy assessments is given by Clapuyt et al. (2015).

A limited number of studies of close-range photogrammetry in glacial and periglacial environments exists, and they principally involve the use of Unmanned Aerial Vehicles (UAVs) for image acquisition (Solbø and Storvold, 2013; Whitehead et al., 2013; Immerzeel et al., 2014; Tonkin et al., 2014; Gauthier et al., 2014; Bühler et al., 2014; Dall'Asta et al., 2015a; Ryan et al., 2015) rather than ground-based surveys (Gómez-Gutiérrez et al., 2014, 2015; Piermattei et al., 2015). Kääb et al. (2014) tested the time-lapse SfM approach in the measurement of vertical and horizontal changes in periglacial patterned grounds.

The objective of our work was to assess the potential and the limits of the ground-based SfM approach in monitoring glacial and periglacial processes in a high-altitude area of the Ortles-Cevedale Group (Eastern Italian Alps). In particular, we used the approach to calculate the geodetic annual mass balance of a 2.1 km^2 glacier and to detect the surface displacement of a neighbouring 0.06 km^2 rock glacier.

The accuracy of the photogrammetric DTMs was estimated using ALS-based DTMs acquired during the same periods. The main factors affecting the accuracy of the pho-

Analysis of glacial and periglacial processes using SfM

L. Piermattei et al.

togrammetric DTMs were investigated, and the significance of the biases in the quantification of glacial and periglacial processes was discussed.

2   Case studies

The La Mare Glacier and the neighbouring AVDM3 Rock Glacier are located in the south-eastern part of the Ortles-Cevedale massif (Eastern Italian Alps), the largest glaciated mountain group of the Italian Alps (Fig. 1).

The La Mare Glacier (World Glacier Inventory code I4L00102517; WGMS 1989) is a 3.55-km^2 valley glacier currently composed of two ice bodies, which have different morphologies and tend to separate (Carturan et al., 2014). In this work we focused on the southern ice body, which feeds the main tongue. This 2.11 km^2 ice body primarily faces north-east, and its surface is rather flat, with the exception of the small remnant of its valley tongue. The elevation ranges from 2660 to 3590 m a.s.l. Mass balance investigations using the direct glaciological method were started on La Mare Glacier in 2003 and detected an average annual mass balance of -0.76 m w.e. y^{-1} during the period from 2003 to 2014 (Carturan, 2015). The mass balance was close to zero in 2013 (-0.06 m w.e.) and was positive for the first time since the beginning of measurements in 2014 ($+0.83$ m w.e.).

The AVDM3 Rock Glacier (Carturan et al., 2015) is an intact, tongue-shaped rock glacier characterized by the presence of two lobes. The 0.058 km^2 wide Rock Glacier (maximum length of 390 m; maximum width of 240 m) faces south-east and is located at elevations of between 2943 and 3085 m a.s.l. The average slope of the Rock Glacier is 26°, and the slope of the advancing front is 36°. The activity status of the AVDM3 Rock Glacier was assessed via repeat geomorphological field surveys between 2007 and 2014. These surveys revealed the advance of the front of the southern lobe (Carturan, 2010). The general morphology and the elevation of the front also suggest that this rock glacier is active (Seppi et al., 2012), and its permafrost content is further corroborated by spring temperature measurements (Carturan et al., 2015). Moreover, Bertone

(2014) provided the first quantification of the surface displacement rates of this rock glacier for 2003 to 2013 using ALS data.

3 Methods

In this section, we briefly describe the ALS data that were used to (i) select the ground control points (GCPs) required to scale and georeference the SfM 3-D models, (ii) co-register the point clouds before producing the DTMs, and (iii) validate the photogrammetric results. Then, we describe how the photogrammetric surveys were performed and processed to produce the dense point clouds and DTMs of the La Mare Glacier and AVDM3 Rock Glacier.

3.1 The ALS data

ALS flights of the study area were available for 17 September 2003, 22 September 2013, and 24 September 2014. The technical specifications of the three ALS surveys are reported in Table 1. To avoid errors due to global shifts or rotations between the individual DTMs, we automatically co-registered the ALS point clouds using a version of the ICP algorithm (Chen and Medioni, 1991; Besl and McKay, 1992) tailored to topographic point clouds (Glira et al., 2015). The lidar point cloud acquired in 2013 was treated as a reference only for stable areas outside the glaciers, rock glaciers, snow patches, and geomorphologically active areas (e.g., landslides, river beds, and debris flows). The 2003 and 2014 lidar point clouds were iteratively fitted to the reference point cloud by applying an affine transformation. The ICP registration of the point clouds produced z-direction residual values of 0.08 and 0.11 m for the 2014 and 2003 lidar point clouds, respectively. These accuracies can be assumed to be sufficient for calculating the annual elevation changes of the glacier and the decadal displacement rate on the rock glacier.

L. Piermattei et al.

The co-registered point clouds were then converted to DTMs using Natural Neighbours interpolations. A pixel size of 1 m × 1 m was produced for the La Mare Glacier, whereas a pixel size of 0.5 m × 0.5 m was used for the rock glacier, based on the lidar point cloud density (Fig. 2). To evaluate the relative ALS DTM accuracies after the co-registration, the elevation difference errors of the DTMs were calculated for the stable areas. The standard deviation from the 2013 ALS DTM was 0.19 and 0.21 m for the 2014 and 2003 DTM comparisons, respectively.

3.2 The photogrammetric workflow

3.2.1 Field surveys

The terrestrial photogrammetric surveys of the La Mare Glacier were conducted on 4 September 2013 and 27 September 2014, that is, close to the end of the mass balance year and of ALS flights. The timing of the surveys enabled the calculation of the annual mass balance of the glacier and the ability to compare the results with the ALS-based results. On both days, the sky was clear, with almost no cloud cover.

To guarantee a safe and easily repeatable survey of the glacier, we avoided directly accessing its surface, instead performing the survey from a rocky ridge on the north side of the glacier (Fig. 4). The elevation of the survey ranged from 3100 to 3300 m in 2013 and from 2600 to 3300 m in 2014. The distance from the glacier surface to the camera positions dictated by the topography ranged between 300 and 2900 m. To cover the entire glacier surface from these positions, the acquired images were panoramic, which involved taking a series of photographs rotating the camera from each individual camera position. In 2013, seven camera positions were used, and 37 photographs were taken with the camera attached to a small tripod to avoid camera shake. In 2014, the number of camera positions was increased to 21, and 177 photos were taken freehand (Fig. 3).

Both surveys were performed using a SLR Canon EOS 600D. The camera was equipped with a 25–70 mm zoom lens, which was set to a focal length of 25 mm in 2013 and 35 mm in 2014.

The terrestrial photogrammetric survey of the AVDM3 Rock Glacier was performed on 27 September 2014. In this survey, 198 images were acquired freehand while walking around and on top of the rock glacier. The survey camera was a CANON EOS 5D full frame SLR camera equipped with a fixed-focal lens of 28 mm. The photographs were acquired and saved in RAW format in both surveys.

3.2.2 Data processing

The latest evolution of photogrammetry is characterized by the combination of the principles of photogrammetry, such as bundle adjustment, and automatic computer vision algorithms, such as feature extraction and feature matching. This photogrammetric approach, called Structure from Motion (SfM), can automatically derive the 3-D position of an object in images taken in sequence calculating the camera parameters (intrinsic and extrinsic) (Hartley and Zissermann, 2004). Dense image matching algorithms are then used to reconstruct the 3-D model of the object as a dense point cloud. Multiple photogrammetric packages implementing SfM and Multi-View Stereo (MVS) algorithms for dense image matching exist, and in this work, we used the software PhotoScan Pro (AgiSoft LLC. 2010a). Henceforth, we refer to the photogrammetric surveys and results using the acronym SfM-MVS.

The photo-based reconstruction workflow is summarized in Fig. 4. The key components of the workflow are (1) acquisition and photograph editing, (2) GCPs identification, image feature detection, matching and 3-D scene reproduction (the SfM-MVS steps), (3) point cloud processing, (filtering, subsampling and ICP) and (4) DTM reconstruction.

To overcome the significant variability in brightness during the surveys, the RAW images have been edited to adjust the exposure and contrast in order to retrieve information from the overexposed (e.g., snow-covered) areas and underexposed (e.g.,

shadowed) areas. These editing steps had a positive impact on the number of image features extracted. The edited images were saved in TIFF format and loaded in PhotoScan where non-stationary objects (i.e., clouds and shadows), the sky, and features lying in the distant background have been masked.

5   The camera calibration parameters were calculated using artificial targets prior to the processing of the photogrammetric surveys (pre-calibrated camera). The intrinsic parameters were kept constant during the entire SfM processing given the limits of the camera network geometry and the homogeneous texture of the surveyed terrain. As additional constraint, the GCPs were included into the SfM process to avoid instability 10 in the bundle adjustment solution (Verhoeven et al., 2015). The GCPs were selected as natural features in stable area outside the glacier and rock glacier, and their co-ordinates were extracted from the 2013 ALS hillshaded DTM. After the SfM step, the geo-referenced dense point cloud was reconstructed by the MVS algorithm, using the "mild" smoothing filter to preserve as much spatial information as possible (AgiSoft 15 LLC., 2010b).

    To reduce the noise and outliers generated during the dense matching reconstruction (Bradley et al., 2008; Nilosek et al., 2012), an initial filtering was performed in PhotoScan to manually remove the outliers. Further denoising was applied to the dense point clouds exported from PhotoScan, using a specific tool to treat the point clouds. 20 To obtain a uniform spatial distribution of the points, the photogrammetric point clouds (much denser than the ALS point clouds), were down-sampled to 20 cm for the glacier and 10 cm for the rock glacier. Following the same procedure used for the ALS data, the ICP algorithm (OpalsICP, TU Vienna) was applied to co-register the point clouds in the stable area outside the glacier and rock glacier, using the 2013 ALS point cloud as 25 a reference. The co-registered point clouds were then converted to DTMs, using the Natural Neighbours interpolation and the pixel sizes of the ALS DTMs (i.e., 1 m × 1 m for the glacier and 0.5 m × 0.5 m for the rock glacier). The data acquisition settings and processing results of the photogrammetric surveys are summarized in Table 2.

3.3 Analyses

The accuracy of the photogrammetric DTMs was assessed to calculate the mean and the standard deviation (σ) of the elevation differences (DTM of Difference, DoD) between SfM-MVS DTMs and ALS DTMs, using the latter as a reference dataset. For both surveyed areas, the primary factors controlling the quality of the photogrammetric DTMs (i.e., camera–object distance, slope and angle of incidence, camera network geometry, surface texture and shadows) were evaluated in terms of DTM accuracy and spatial resolution. After the accuracy assessments, we investigated the suitability of using the terrestrial photogrammetric surveys to calculate the annual mass balance of the glacier and the surface displacement rates of the rock glacier, comparing the results with those obtained from ALS surveys.

4 Results

4.1 Accuracy assessment on the area of La Mare Glacier

The mean elevation difference between the SfM-MVS DTM from 4 September 2013 (Fig. 5a) and the ALS DTM from 22 September 2013 (Fig. 2b), evaluated in the common stable area outside the glacier, was −0.42 m ($\sigma = 1.72$ m). The same calculation between the SfM-MVS DTM from 27 September 2014 (Fig. 5b) and the ALS DTM from 24 September 2014 (Fig. 2a) yielded a mean value of 0.03 m ($\sigma = 0.74$ m). In this area, the mean difference between the 2014 and 2013 SfM-MVS DTMs is 0.38 m ($\sigma = 1.73$ m), and the mean difference between the respective ALS DTMs is −0.09 m ($\sigma = 0.29$ m, Table 3).

These results show that the photogrammetric survey conducted in 2014, using a higher number of camera positions and photographs and a slightly longer focal length, provided a significant improvement compared to the survey of 2013. In addition to the

higher σ, the 2013 SfM-MVS DTM has a residual average bias of −0.42 m, which must be taken into account in the glacier mass balance calculations.

Table 3 also presents the same statistics for the area of the glacier. However, given that in 2013 the ablation was not negligible between the photogrammetric survey of 4 September and the ALS survey of 22 September, the comparison between SfM-MVS and ALS of the same year is meaningful only in 2014, with a mean difference of 0.23 m ($\sigma = 0.65$ m). The comparison of the two ALS DTMs of 2014 and 2013 yields a mean difference of 1.30 m for the glacier, attributable to the positive mass balance experienced by the glacier in that time period (+0.83 m w.e., Carturan, 2015).

The spatial distribution of the elevation difference between the SfM-MVS and ALS DTMs surveyed at the same times (Figs. 6 and 7) suggests that the most problematic areas for photogrammetric reconstructions are those that are far from the camera positions, steep, and covered by fresh snow. Certain outliers can be observed in steep areas outside the glaciers, even after filtering, but they likely have no influence on the glacier, where the slope is much lower. Using the SfM-MVS DTM from 27 September 2014, which has a higher spatial coverage than that of 2013 and is almost contemporaneous with the ALS DTM from 24 September 2014 (which means negligible ablation and accumulation on the glacier), we investigated in detail the factors controlling the quality of the photogrammetric DTMs.

As expected, the standard deviation of elevation differences between the 2014 SfM-MVS and ALS DTMs is proportional to slope but remains lower than 1 m up to 40° on the glacier and up to 60° in the area outside it (Fig. 8). A rapid increase in the error is observed for the highest slope classes, which represent a very small part of the investigated area. For the glacier, only 1 % of the area has a slope higher than 40°. The mean elevation difference is around zero for most of the low- and middle-slope classes, with the exception of the 0–10° class inside the glacier, where a mean value of 0.41 m ($\sigma = 0.44$ m) was calculated. The majority of this slope class lies in a flat area of the glacier at 3200–3300 m a.s.l. and is covered by fresh snow. In addition, this zone has an unfavourable line of sight from the camera positions.

We therefore investigated the role of the incidence angle between the line of sight of the camera and the photographed object (vector normal to the surface), analysing five camera locations at different elevations. As Fig. 9a shows, more than 80 % of the incidence angles in single pixels range between 70 and 90˚. Figure 9c shows no statistically significant relationship between incidence angle and elevation difference confirming the conclusions reached by Piermattei et al. (2015). Contrary to what was speculated, high mean and standard deviation values were obtained for low (i.e., theoretically favourable) incidence angles, which correspond to areas with high slope. Instead, low and approximately constant low standard deviation values were obtained for high incidence angles. These results suggest that, in our case study, the accuracy of the SfM-MVS DTMs is influenced more by the slope than by the incidence angle.

Because the camera–object distance (depth) strongly influences the photogrammetric accuracy (Gómez-Gutiérrez et al., 2014), we evaluated its effect by calculating the mean and standard deviation of the elevation difference between the 2014 SfM-MVS and ALS DTMs, clustering the pixels in 200 m distance classes from a camera position at the centre of the array displayed in Fig. 4b. The relationship between error and depth is clearer for the glacier area (Fig. 10a), whereas in the surrounding area, the error appears to be more influenced by the variability of the slope angle (Fig. 10b).

The obtained results were compared to the theoretical behaviour of the error as a function of the depth (σ_d), as calculated using the following formulation:

$$\sigma_d = m_B \cdot \frac{D}{B} \cdot \sigma_i, \tag{1}$$

where m_B represents the image scale (D/focal length); D is the depth (camera–object distance); B is the baseline and σ_i is the measured accuracy in the image space.

The theoretical σ_d was calculated for each class of distance considering a mean baseline of 400 m and an accuracy in the image space of 0.40 pixel, which is the reprojection error after bundle adjustment computations. Another quantification of the error as a function of the depth was obtained, for comparison purposes, by multiplying the Ground Sample Distance (GSD) (which increases with depth) by the reprojection

error provided by PhotoScan for the Ground Control Points. Figure 10c shows that, on the glacier, the accuracy calculated from the DoD matches quite well the "theoretical" calculations up to a depth of 1900 m. Beyond this distance, the detected error increases faster than in theory, likely due to the increasing coverage of fresh snow, which affects the image texture and decreases the accuracy.

We then investigated the accuracy of photogrammetric reconstruction for the different substrata, whose spatial distribution was outlined on the orthophoto exported from PhotoScan. Debris, ice and firn display similar accuracy, with median values of elevation difference between the 2014 SfM-MVS and ALS-based DTMs close to zero and interquartile ranges of the same magnitude. Conversely, the area covered by fresh snow, which is also the area with greater depth, shows prevailing positive differences, a median value of 0.48 m and a much higher standard deviation ($\sigma = 0.82$ m).

The texture of the surface also influences the point density distribution and the spatial coverage of the reconstructed area. A lower value of the point density was obtained for fresh snow (4 pts m^{-2}). Increasing point densities were obtained for firn, ice and debris (10, 13 and 15 pts m^{-2}, respectively).

The spatial coverage in the fresh snow area was 75 %, whereas it was 93 % in the rest of the glacier. Excluding the areas not visible from the camera position and occlusions imposed by the topography, the spatial coverage in the fresh snow area was 82 and 98 % in the remaining part.

The point density is also affected by the depth, elevation and slope (Fig. 12). Due to the GSD, the average point density decreases with depth, which in our case is also proportional to the elevation. On the glacier, the point density decreases more rapidly than in the surrounding area for elevations between 3100 and 3300 m a.s.l., due to the poor texture in this snow-covered flat area. Increasing densities with slope, up to 70–80°, are observed and likely result from more favourable incidence angles, which do not however guarantee high accuracy, as noted earlier (Fig. 9). Considering the entire reconstructed surface, the point density was higher in the area surrounding the glacier than on it (12 pts m^{-2} vs. 8 pts m^{-2}, respectively).

4.2 Accuracy assessment in the area of the AVDM3 Rock Glacier

The 2014 terrestrial photogrammetric survey of the AVDM3 Rock Glacier provided a good spatial coverage (83 %) of high-resolution terrain data (Fig. 13). The spatial distribution of the elevation difference between the contemporaneous SfM-MVS and ALS DTMs shows the existence of areas with both positive and negative values (Fig. 14). The average elevation difference is 0.02 m on the rock glacier ($\sigma = 0.17$) and 0.05 in the surrounding areas ($\sigma = 0.31$ m, Table 5).

Similar to the La Mare Glacier area, the accuracy decreases with increasing slope in the rock glacier area. The standard deviation of the average elevation difference between the SfM-MVS and ALS DTMs is less than 0.20 m up to 40°. In the area surrounding the rock glacier, the error increases faster with slope because steep areas coincide with shaded areas and (because the images were acquired in the afternoon) high solar zenith angles. As suggested by Gómez-Gutiérrez et al. (2014), we calculated the relationship between the quality of the photogrammetric DTM and the amount of shadowed-lighted areas in the photographs, using a hillshaded model that was calculated by simulating the position of the sun in the sky (azimuth and zenith angles) during the survey. As shown in Fig. 16, larger errors occur in shadowed areas and smaller errors in well-lit areas, even if the largest differences in accuracy can be observed outside rather than on the rock glacier.

4.3 Glacial and periglacial processes

4.3.1 Mass balance calculations on La Mare Glacier

Due to abundant solid precipitation during the accumulation season and low ablation rates during the summer (the glacier was snow-covered above $\sim$ 3000–3100 m a.s.l.), the mass balance of the La Mare Glacier was positive in the 2013–2014 hydrological year for the first time since the beginning of measurements in 2003. At the end of the ablation season, the Equilibrium Line Altitude (ELA) was at 3012 m a.s.l., and the

Accumulation Area Ratio (i.e., the ratio between the accumulation area and the total area, AAR) was 0.86. According to the direct glaciological method, the annual mass balance was +0.83 m w.e. (Carturan, 2015).

We compared mass balance estimates obtained with the geodetic method based on the SfM-MVS and ALS DTMs acquired in 2013 and 2014. The geodetic mass balance was calculated from the total volume change ΔV (m^3) between the two survey dates:

$$V = \overline{\Delta z} \cdot A \tag{2}$$

where $\overline{\Delta z}$ is the average elevation change between two DTMs over the area A of the glacier. The area-averaged net geodetic mass balance in metres of water equivalent per year (m w.e.y^{-1}) was calculated as

$$\dot{M} = \frac{\Delta V \cdot \rho}{A} \tag{3}$$

where ρ is the mean density. The area A of the glacier between the two surveys did not change. The mean density was obtained by a fractional area-weighted mean, assigning 900 kg m^{-3} for the ablation area (Huss, 2013) and 530 kg m^{-3} for the accumulation area, as directly measured in a snowpit. The resulting weighted mean density was 600 kg m^{-3}. In the mass balance calculations, we used both raw $\overline{\Delta z}$ values and corrected $\overline{\Delta z}$ values to account for the mean errors in the stable areas outside the glacier, as reported in Table 3.

As shown in Table 4, the geodetic mass balance estimates using only ALS data do not differ significantly for either the entire glacier or the sub-areas covered by the photogrammetric surveys of 2013 and 2014 (88 and 93 %, respectively). The estimates range between 0.85 and 0.88 m w.e. for the raw data and between 0.90 and 0.94 m w.e. for the corrected data. The geodetic mass balance calculations using only photogrammetric data yield a raw value of 1.09 m w.e. and a corrected value of 0.87 m w.e. Using the 2014 SfM-MVS, which has a higher quality than the 2013 ALS DTM, yields a raw

value of 0.98 m w.e. and a corrected value of 1.02 m w.e. Area-averaged estimates of the geodetic mass balance from photogrammetric data are very close to the estimates from ALS data and from the direct method and are closer still if the mean DTM error in the stable areas outside the glacier is subtracted from the raw average elevation differ-
5 ences. The spatial distribution and magnitude of elevation change is also well captured by the terrestrial photogrammetry (Figs. 17 and 18), even if, as already noted in the previous section, problematic areas are present in the upper part of the glacier, which was covered by fresh snow, especially in the 2013 SfM-MVS survey.

4.3.2 Surface changes and velocities of the AVDM3 Rock Glacier

10 The spatial distribution and the mean value of elevation change on the surface of the AVDM3 Rock Glacier were calculated differencing the available SfM-MVS and ALS DTMs. Table 5 shows that, according to the ALS data, there was a prevailing lowering of the surface in the period from 2003 to 2014. Taking into account the average residual bias in the stable area outside the rock glacier, the average lowering rates of the rock
15 glacier surface were 1.5 cm y^{-1} in the period from 2003 to 2013, and 2 cm in the year 2013–2014. Comparing the SfM-MVS DTM of 2014 with the ALS DTMs of 2013 and 2003 and accounting for the mean bias outside the rock glacier, we obtained slightly higher lowering rates of 2.2 cm y^{-1} from 2003 to 2013 and 5 cm from 2013 to 2014. As expected on the basis of the accuracy assessment (Sect. 4.2), the decadal lowering
20 rates calculated from the SfM-MVS DTM are in closer agreement with those calculated from ALS data than the single-year calculations. The same can be observed for the spatial distribution of the elevation changes (Fig. 19), which shows a prevailing thinning in the upper and middle part of the rock glacier and a thickening of the two advancing lobes.
25 Based on these results, we compared the surface displacement rates (based on photogrammetric and ALS data) for the period from 2003 to 2014. We used manual measurements of the displacement of single boulders identified in the hillshaded DTMs.

L. Piermattei et al.

Several points were also located outside the rock glacier to assess the accuracy of the surface velocity determinations.

Figure 20 shows that the fastest moving areas are the two frontal lobes, which also featured the greatest elevation changes. Table 6 shows that the SfM-MVS and ALS data produced very similar surface velocities for the three sub-areas (each with homogeneous displacement) into which the rock glacier can be divided. Outside the rock glacier, the photogrammetric method exhibited a slightly lower accuracy compared to the ALS, but no systematic shift of the different DTMs was found.

5   Discussion

The results of our terrestrial photogrammetry applications on the La Mare Glacier and on the AVDM3 Rock Glacier demonstrate that it is possible to reliably quantify the investigated glacial and periglacial processes by means of a quick and safe survey that was conducted on a single day using cheap, light and easy-to-use hardware. Moreover, time-consuming and unsafe direct access to the glacier surface was not required.

However, the data processing times were significantly longer. For a single operator, the processing time is approximately 10 days. The most labour-intensive and time-consuming tasks were the pre-processing steps i.e., masking of the photos, identification of reference points from the lidar DTM and then in the images, and processing of the images (the MVS step is particularly computationally intensive), which is directly related to the resolution and the number of photographs uploaded and the computer performance. Several steps required a certain degree of subjectivity, e.g., the identification of the GCPs. However, due to the high automatism of the image processing, the level of expertise is considerably lower than for lidar and traditional photogrammetry.

On the La Mare Glacier, the area-averaged estimates of the 2013–2014 geodetic mass balance from ALS and photogrammetric data were almost identical (0.91 and 0.87 m w.e., respectively) and close to the mass balance calculated from the direct glaciological method (0.83 m w.e.). The differences are well within the uncertainty

of the direct mass balance estimates, which has been quantified as approximately $\pm 0.2\,\mathrm{m\,w.e.\,y}^{-1}$ by previous studies (Cogley and Adams, 1998; Cogley, 2009). These results confirm that the good results obtained by Piermattei et al. (2015) on the small Montasio Glacier, in the Julian Alps, can also be replicated on larger glaciers with different morphologies and characteristics.

Because the AVDM3 Rock Glacier exhibited quite slow annual deformation and creep, we were able to calculate reliable displacement rates and area-averaged surface elevation changes only on a multi-year (in our case, decadal) time scale. This result confirms the findings of Gómez-Gutiérrez et al. (2014), who applied a similar method to the Corral del Veleta Rock Glacier in the Sierra Nevada (Spain).

Our results are promising, despite the limitations of the adopted expeditious method, which include (i) the location of GCPs on natural targets outside the investigated glacier/rock glacier, (ii) the presence of areas with deep shadows and changes in the light during the survey, (iii) the presence of fresh snow in the upper and middle part of the glacier, and (iv) the high camera–object distance in the glacier application.

In general terms, the photo-based accuracy is related to the image feature extraction, feature matching (in both the SfM and MVS steps), and scale definition (Bemis et al., 2014). A low accuracy in these steps, caused for example by poor camera network geometry, can generate model distortion and reduce the ability to identify unique corresponding features in overlapping images (Wackrow and Chandler, 2011; Dall'Asta et al., 2015b; Favalli et al., 2012; James and Robson, 2014; Hosseininaveh et al., 2014; Nocerino et al., 2014). In our case studies, among the various aspects analysed, the spatial variability of the accuracy of the photogrammetric DTMs is related to the camera–object distance, the presence of fresh snow with low contrast, the changing illumination during the survey and the occurrence of shadows. The increasing error with increasing terrain slope suggests the persistence of a small shift in the reconstructed DTMs. This shift, however does not affect the areal estimates of mass balance and elevation change, given that the vast majority of the glacier and rock glacier areas feature small or moderate slope angles. For both the glacier and the rock glacier, we have not

obtained complete spatial coverage. In the glacier surveys, the problematic areas were those not visible from the camera positions and those covered by fresh snow and far from the viewpoints. In the rock glacier, certain areas were not reconstructed due to the rock glacier's complex morphology and in particular to the presence of ridges, furrows and counterslopes.

Our accuracy assessments confirm that the ALS data still provide results with somewhat higher accuracies (Tables 3 and 5, Figs. 6 and 14) but with much higher costs and demanding logistics than the SfM-MVS approach. However, the SfM-MVS method has the potential to provide a significantly higher spatial resolution (Debella-Gilo and Kaab, 2011; Piermattei et al., 2015) and temporal resolution due to its significantly lower costs. Moreover, the photogrammetric reconstructions still have room for improvement, as demonstrated by the better results achieved from the 2014 survey of the glacier area compared to those from 2013. This improvement resulted from a higher number of photographs and improved camera network geometry.

Many of the limitations described above can be overcome by introducing modifications to the terrestrial photogrammetric survey strategy. For the rock glacier survey, shorter baselines are recommended to ensure greater spatial coverage, high image similarity and good matching performance (Wenzel et al., 2013). GCPs, for example, could be placed on the surface of the glaciers and rock glaciers to reduce the model distortions (Bemis et al., 2014) and generate surveys with much higher accuracies via, for example, the use of dGPS (Dall'Asta et al., 2015a).

The use of Unmanned Aerial Vehicles (UAVs) could solve the problem of excessive camera–object distances and the issue of missing areas due to inaccessibility. However, these alternatives imply increased costs, more troublesome logistics, greater expertise, and ultimately longer survey times. In addition, they also require directly accessing unsafe or difficult to reach areas, both to place targets and to move UAVs among study areas that exceed their operational range (Bühler et al., 2014). Therefore, the best balance must be found between simplicity, safety, costs and accuracy for each

photogrammetric application based on the final objectives and on the available human and economic resources.

6 Conclusions

In this paper, we investigated the applicability of the SfM-MVS approach for monitoring glacial and periglacial processes in a catchment of the Ortles-Cevedale Group (Eastern Italian Alps), validating our results using ALS DTMs as benchmarks. The ground surveys were conducted on foot and were intentionally planned to be as quick and easy as possible. We surveyed the 2.1 km^2 La Mare Glacier and the neighbouring AVDM3 Rock Glacier in one day using only a consumer-grade SLR camera without the setup of artificial targets.

The accuracy of the photogrammetric DTMs, evaluated as the mean and standard deviation of the elevation difference in a stable area between the SfM-MVS DTM and the reference ALS DTM, was -0.42 ± 1.72 m and 0.03 ± 0.74 m for the 2013 and 2014 surveys, respectively. The SfM-MVS DTM accuracy of the reconstructed rock glacier surface acquired in 2014 was estimated to be 0.02 ± 0.17 m.

The SfM-MVS geodetic mass balance estimates for the La Mare Glacier were in good agreement with the calculations from the contemporary ALS data and with the results of the direct glaciological method, confirming a positive mass balance of approximately 0.9 m w.e. in the 2013–2014 hydrological year. In the rock glacier, the expeditious survey produced a good spatial coverage of the photogrammetric DTM and a reliable calculation of the multi-year surface changes and displacement rates. For rock glacier applications, particularly for slow-mowing ones such as AVDM3, single-year assessments of elevation change and surface velocities require the setup of artificial targets and GCPs to obtain the accuracy required to detect such slow processes.

The simplicity of the ground surveys and the physical characteristics of the analysed alpine terrain were the main factors influencing the tested approach. In particular, we refer to the use of natural targets as GCPs, the occurrence of shadowed areas and

lighting changes during the surveys, the presence of fresh snow in the upper part of the glacier (which reduced the contrast), and the sub-optimal camera network geometry and long camera–object distances imposed by the morphology and accessibility of the study area.

In consideration of the factors that spatially control the accuracy of the SfM-MVS DTMs, there remains room for significant improvements, e.g., using UAVs and/or placing artificial targets surveyed by dGPS. Further research is therefore needed to (i) find technical solutions to overcome the major limitations of the SfM-MVS approach in such remote areas and (ii) achieve the optimal balance between the simplicity and low cost of this approach and the accuracy required for each specific application.

References

Abermann, J., Fischer, A., Lambrecht, A., and Geist, T.: On the potential of very high-resolution repeat DEMs in glacial and periglacial environments, The Cryosphere, 4, 53–65, doi:10.5194/tc-4-53-2010, 2010.

AgiSoft LL C: AgiSoft PhotoScan Professional Edition. Version 1.1.2, available at: http://www.agisoft.ru/products/photoscan/ (last access: 18 January 2015), 2010a.

AgiSoft LL C: AgiSoft PhotoScan User-manuals Version 1.0, available at: http://www.agisoft.com/pdf/photoscan-pro_1_1_en.pdf (last access: 15 May 2015), 2010b.

Aguilar, F. J. and Mills, J.: Accuracy assessment of lidar-derived digital elevation models, Photogramm. Rec., 23, 148–169, 2008.

Ahn, Y. and Box, J., E.: Glacier velocities from time-lapse photos: technique development and first results from the Extreme Ice Survey (EIS) in Greenland. J. Glaciol., 56, 723–734, 2010.

Baltsavias, E. P., Favey, E., Bauder, A., Bosch, H., and Pateraki, M.: Digital surface modelling by airborne laser scanning and digital photogrammetry for glacier monitoring, Photogramm. Rec., 17, 243–273, doi:10.1111/0031-868X.00182, 2001.

Bemis, S., Micklethwaite, S., and Turner, D.: Ground-based and UAV-Based photogrammetry: a multi-scale, high-resolution mapping tool for Structural Geology and Paleoseismology. J Struct Geol., 69, 163–178, doi:10.1016/j.jsg.2014.10.007, 2014.

Bertone, A.: Misure di spostamento dei rock glacier con l'uso di feature tracking applicato a DTM multitemporali, BSc Thesis, Department of Earth and Environmental Sciences, University of Pavia, Pavia, Italy, 63 pp., 2014.

Besl, P. J. and McKay, N. D.: Method for registration of 3-D shapes, in: Proceedings of the International Society for Optics and Photonics IEEE Transactions on Pattern Analysis and Machine Intelligence, 1611, 586–606, 1992.

Bradley, D., Boubekeur, T., and Heidrich, W.: Accurate multi-view reconstruction using robust binocular stereo and surface meshing, in: IEEE Conference on Computer Vision and Pattern Recognition, Anchorage, AK, USA, 1–8, 2008.

Bühler, Y. and Graf, C.: Sediment transfer mapping in a high-alpine catchment using airborne LiDA R. GRAF, C.(Red.) Mattertal – ein Tal in Bewegung, Publikation zur Jahrestagung der Schweizerischen Geomorphologischen Gesellschaft, 29 June–1 July 2011, Eidg. Forschungsanstalt WSL, St. Niklaus, Birmensdorf, Switzerland, 113–124, 2013.

Bühler, Y., Marty, M., Egli, L., Veitinger, J., Jonas, T., Thee, P., and Ginzler, C.: Spatially continuous mapping of snow depth in high alpine catchments using digital photogrammetry, The Cryosphere Discuss., 8, 3297–3333, doi:10.5194/tcd-8-3297-2014, 2014.

Carturan, L.: Climate change effects on the cryosphere and hydrology of a high-altitude watershed, PhD thesis, Department of Land, Environment, Agriculture and Forestry, University of Padova, Padova, Italy, 2010.

Carturan, L.: Starting new mass balance observations close to decaying monitored glaciers: La Mare Glacier (Ortles-Cevedale, Italian Alps), J. Glaciol., in preparation, 2015.

Carturan, L., Cazorzi, F., and Dalla Fontana, G.: Enhanced estimation of glacier mass balance in unsampled areas by means of topographic data, Ann. Glaciol., 50, 37–46, 2009.

Carturan, L., Baldassi, G., Bondesan, A., Calligaro, S., Carton, A., Cazorzi, F., Dalla Fontana, G., Francese, R., Guarnieri, A., Milan, N., Moro, D., Tarolli, P.: Current behavior and dynamics of the lowermost italian glacier (Montasio Occidentale, Julian Alps), Geografiska Annaler: Series A, Physical Geography, 95, 79–96, 2013.

Analysis of glacial and periglacial processes using SfM

L. Piermattei et al.

Title Page

Abstract	Introduction
Conclusions	References
Tables	Figures

◄◄	►►
◄	►
Back	Close

Full Screen / Esc

Printer-friendly Version

Interactive Discussion

Carturan, L., Baroni, C., Carton, A., Cazorzi, F., Fontana, G. D., Delpero, C., and Zanoner, T.: Reconstructing Fluctuations of La Mare Glacier (Eastern Italian Alps) in the Late Holocene: new Evidence for a Little Ice Age Maximum Around 1600 AD. Geografiska Annaler: Series A, Physical Geography, 96, 287–306, 2014.

Carturan, L., Zuecco, G., Seppi, R., Zanoner, Z., Borga, M., Carton, A., and Dalla Fontana, G.: Catchment-scale permafrost mapping using spring water characteristics, Permafrost Periglac., in press, 2015.

Chen, Y. and Medioni, G.: Object modeling by registration of multiple range images, in: Proceedings, IEEE International Conference on Robotics and Automation, 9–11 April, Sacramento, CA, USA, 10, 145–155, 1991.

Clapuyt, F., Vanacker, V., and Van Oost, K.: Reproducibility of uav-based earth topography reconstructions based on structure-from-motion algorithms, Geomorphology, doi:10.1016/j.geomorph.2015.05.011, 2015.

Cogley, J. G.: Geodetic and direct mass-balance measurements: comparison and joint analysis, Ann. Glaciol., 50, 96–100, 2009.

Cogley, J. G. and Adams, W. P.: Mass balance of glaciers other than the ice sheets, J. Glaciol., 44, 315–325, 1998.

Colucci, R. R., Forte, E., Boccali, C., Dossi, M., Lanza, L., Pipan, M., and Guglielmin, M.: Evaluation of internal structure, volume and mass of glacial bodies by integrated LiDAR and ground penetrating radar surveys: the case study of Canin Eastern Glacieret (Julian Alps, Italy), Surv. Geophys., 36, 231–252, 2015.

Dall'Asta, E., Delaloye, R., Diotri, F., Forlani, G., Fornari, M., Morra di Cella, U., Pogliotti, P., Roncella, R., Santise, M.: Use of UAS in a high mountain landscape: the case of gran sommetta rock glacier (AO), The International Archives of the Photogrammetry, Remote Sensing and Spatial Information Sciences, Volume XL-3/W3, 391–397, 2015a.

Dall'Asta, E., Thoeni, K., Santise, M., Forlani, G., Giacomini, A., and Roncella, R.: Network design and quality checks in automatic orientation of close-range photogrammetric blocks, Sensors, 15, 7985–8008, 2015b.

Debella-Gilo, M. and Kääb, A.: Sub-pixel precision image matching for measuring surface displacements on mass movements using normalized cross-correlation. Remote Sens. Environ., 115, 130–142, 2011.

Deems, J. S., Painter, T. H., and Finnegan, D. C.: Lidar measurement of snow depth: a review, J. Glaciol., 59, 467–479, 2013.

Analysis of glacial and periglacial processes using SfM

L. Piermattei et al.

Title Page

Abstract | Introduction

Conclusions | References

Tables | Figures

|◄ | ►|

◄ | ►

Back | Close

Full Screen / Esc

Printer-friendly Version

Interactive Discussion

Favalli, M., Fornaciai, A., Isola, I., Tarquini, S., and Nannipieri, L.: Multiview 3D reconstruction in geosciences, Comput. Geosci., 44, 168–176, 2012.

Fischer, L., Eisenbeiss, H., Kääb, A., Huggel, C., and Haeberli, W.: Monitoring topographic changes in a periglacial high-mountain face using high-resolution DTMs, Monte Rosa East Face, Italian Alps, Permafrost Periglac., 22, 140–152, 2011.

Gauthier, D., Conlan, M., and Jamieson, B.: Photogrammetry of fracture lines and avalanche terrain: potential applications to research and hazard mitigation projects, Proceedings, International Snow Science Workshop, Banff, 29 September–3 October 2014, 109–115, , 2014.

Geist, T. and Stotter, J.: Documentation of glacier surface elevation change with multi-temporal airborne laser scanner data – case study: Hintereisferner and Kesselwandferner, Tyrol, Austria, Zeitschrift fur Gletscherkunde und Glazialgeologie, 41, 77–106, 2007.

Glira, P., Pfeifer, N., Briese, C., Ressl, C.: A correspondence framework for ALS strip adjustments based on variants of the ICP algorithm, Photogramm. Fernerkun., 4, 275–289, doi:10.1127/pfg/2015/0270, 2015.

Gómez-Gutiérrez, Á., de Sanjosé-Blasco, J. J., de Matías-Bejarano, J., and Berenguer-Sempere, F.: Comparing two photo-reconstruction methods to produce high density point clouds and DEMs in the Corral del Veleta Rock Glacier (Sierra Nevada, Spain), Remote Sensing, 6, 5407–5427, 2014.

Gómez-Gutiérrez, Á., de Sanjosé-Blasco, J. J., Lozano-Parra, J., Berenguer-Sempere, F., and de Matías-Bejarano, J.: Does HDR pre-processing improve the accuracy of 3D models obtained by means of two conventional SfM-MVS software packages? The case of the Corral del Veleta Rock Glacier, Remote Sensing, 7, 10269–10294, 2015.

Hartley, R. and Zisserman, A.: Multiple View Geometry In Computer Vision, Cambridge University Press, Cambridge, UK, 2003.

Haeberli, W.: Creep of mountain permafrost: internal structure and flow of alpine rock glaciers, Mitteilungen der Versuchsanstalt für Wasserbau, Hydrologie und Glaziologie der ETH Zurich, 77, 5–142, 1985.

Haug, T., Rolstad, C., Elvehøy, H., Jackson, M., and Maalen-Johansen, I.: Geodetic mass balance of the western Svartisen ice cap, Norway, in the periods 1968–1985 and 1985–2002, Ann. Glaciol., 50, 119–125, 2009.

Höfle, B. and Rutzinger, M.: Topographic airborne LiDAR in geomorphology: a technological perspective, Zeitschrift für Geomorphologie, Supplementary Issues, 55, 1–29, 2011.

Höfle, B., Geist, T., Rutzinger, M., and Pfeifer, N.: Glacier surface segmentation using airborne laser scanning point cloud and intensity data, International Archives of Photogrammetry, Remote Sensing and Spatial Information Sciences, 36, W52, 195–200, 2007.

Hosseininaveh, A., Sargeant, B., Erfani, T., Robson, S., Shortis, M., Hess, M., and Boehm, J.: Towards fully automatic reliable 3D acquisition: from designing imaging network to a complete and accurate point cloud, Robotics and Autonomous Systems, 62, 1197–1207, 2014.

Huss, M.: Density assumptions for converting geodetic glacier volume change to mass change, The Cryosphere, 7, 877-887, doi:10.5194/tc-7-877-2013, 2013.

Immerzeel, W. W., Kraaijenbrink, P. D. A., Shea, J. M., Shrestha, A. B., Pellicciotti, F., Bierkens, M. F. P., and De Jong, S. M.: High-resolution monitoring of Himalayan glacier dynamics using unmanned aerial vehicles, Remote Sens. Environ., 150, 93–103, 2014.

James, M. R. and Robson, S.: Straightforward reconstruction of 3D surfaces and topography with a camera: accuracy and geoscience application, J. Geophys. Res.-Earth, 117, F03017, doi:10.1029/2011JF002289, 2012.

James, M. R. and Robson, S.: Mitigating systematic error in topographic models derived from UAV and ground-based image networks, Earth Surf. Proc. Land. 39, 1413–1420, doi:10.1002/esp.3609, 2014.

Joerg, P. C. and Zemp, M.: Evaluating Volumetric Glacier Change Methods Using Airborne Laser Scanning Data. Geografiska Annaler: Series A, Physical Geography, 96, 135–145, 2014.

Kääb, A.: Monitoring high-mountain terrain deformation from repeated air-and spaceborne optical data: examples using digital aerial imagery and ASTER data. ISPRS Journal of Photogrammetry and remote sensing, 57, 39–52, 2002.

Kääb, A.: Remote Sensing of Mountain Glaciers and Permafrost Creep. Research Perspectives from Earth Observation Technologies and Geoinformatics, Schriftenreihe Physische Geographie, Glaziologie und Geomorphodynamik, 48, University of Zurich, Zurich, Switzerland, 2005.

Kääb, A. and Funk, M.: Modelling mass balance using photogrammetric and geophysical data: a pilot study at Griesgletscher, Swiss Alps. J. Glaciol. 45, 575–583, 1999.

Kääb, A., Haeberli, W., and Gudmundsson, G. H.: Analyzing the creep of mountain permafrost using high precision aerial photogrammetry: 25 years of monitoring Gruben rock glacier, Swiss Alps, Permafrost Periglac., 8, 409–426, 1997.

Title Page

Abstract | Introduction

Conclusions | References

Tables | Figures

|◀ | ▶|

◀ | ▶

Back | Close

Full Screen / Esc

Printer-friendly Version

Interactive Discussion

Kääb, A., Kaufmann, V., Ladstädter, R., and Eiken, T.: Rock glacier dynamics: implications from high-resolution measurements of surface velocity fields, in: Eighth International Conference on Permafrost, 21–25 July 2003, Zurich, Switzerland, Vol. 1, 501–506, 2003.

Kääb, A., Girod, L., and Berthling, I.: Surface kinematics of periglacial sorted circles using structure-from-motion technology, The Cryosphere, 8, 1041–1056, doi:10.5194/tc-8-1041-2014, 2014.

Kaufmann, V.: Deformation analysis of the Doesen rock glacier (Austria), in: Proceedings of the 7th International Permafrost Conference, 23–27 June 1998, Yellowknife, Canada, 551–556, 1998.

Kaufmann, V. and Ladstädter R.: Application of terrestrial photogrammetry for glacier monitoring in Alpine environments, Proceedings of the 21st Congress of ISPRS, Beijing, China, 3–11 July 2008, Vol. 37, Part B8, 813–818, 2008.

Knoll, C. and Kerschner, H.: A glacier inventory for South Tyrol, Italy, based on airborne laser-scanner data, Ann. Glaciol., 50, 46–52, 2010.

Kodde, M. P., Pfeifer, N., Gorte, B. G. H., Geist, T., and Höfle, B.: Automatic glacier surface analysis from airborne laser scanning, International Archives of the Photogrammetry, Remote Sensing and Spatial Information Sciences, 36, 221–226, 2007.

Maas, H. G., Schwalbe, E., Dietrich, R., Bässler, M., and Ewert, H.: Determination of spatio-temporal velocity fields on glaciers in West-Greenland by terrestrial image sequence analysis, International Archives of Photogrammetry, Remote Sensing and Spatial Information Science, 37, 1419–1424, 2008.

Micheletti, N., Chandler, J. H., and Lane, S. N.: Investigating the geomorphological potential of freely available and accessible Structure-from-Motion photogrammetry using a smartphone, Earth Surf. Proc. Land., 40, 473–486, doi:10.1002/esp.3648, 2014.

Müller, J., Gärtner-Roer, I., Thee, P., and Ginzler, C.: Accuracy assessment of airborne photogrammetrically derived high-resolution digital elevation models in a high mountain environment. ISPRS Journal of Photogrammetry and Remote Sensing, 98, 58–69, 2014.

Nilosek, D., Sun, S., and Salvaggio, C.: Geo-accurate model extraction from three-dimensional image-derived point clouds, in: Proceedings of SPIE, Algorithms and Technologies for Multi-spectral, Hyperspectral, and Ultraspectral Imagery XVIII, 23 April 2012, Baltimore, MD, USA, 8390, 83900J, doi:10.1117/12.919148, 2012.

Title Page

Abstract | Introduction

Conclusions | References

Tables | Figures

|◄ | ►|

◄ | ►

Back | Close

Full Screen / Esc

Printer-friendly Version

Interactive Discussion

Nocerino, E., Menna, F., and Remondino, F.: Accuracy of typical photogrammetric networks in cultural heritage 3D modeling projects, ISPRS-International Archives of the Photogrammetry, Remote Sensing and Spatial Information Sciences, 1, 465–472, 2014.

Pellikka, P. and Rees, W. G.: Remote Sensing Of Glaciers: Techniques For Topographic, Spatial and Thematic Mapping of Glaciers, CRC Press, University of Cambridge, Cambridge, UK, 2009.

Piermattei, L., Carturan, L., and Guarnieri, A.: Use of terrestrial photogrammetry based on structure from motion for mass balance estimation of a small glacier in the Italian Alps, Earth Surf. Proc. Land., 40, 1791–1802, doi:10.1002/esp.3756, 2015.

Prosdocimi, M., Sofia, G., Dalla Fontana, G., Tarolli, P.: Bank erosion in agricultural drainage networks: effectiveness of Structure-from-Motion for post-event analysis, Earth Surf. Proc. Land., 40, 1891–1906, doi:10.1002/esp.3767, 2015.

Ryan, J. C., Hubbard, A. L., Box, J. E., Todd, J., Christoffersen, P., Carr, J. R., Holt, T. O., and Snooke, N.: UAV photogrammetry and structure from motion to assess calving dynamics at Store Glacier, a large outlet draining the Greenland ice sheet, The Cryosphere, 9, 1–11, doi:10.5194/tc-9-1-2015, 2015.

Roer, I. and Nyenhuis, M.: Rockglacier activity studies on a regional scale: comparison of geomorphological mapping and photogrammetric monitoring, Earth Surf. Proc. Land., 32, 1747–1758, 2007.

Seppi, R., Carton, A., Zumiani, M., Dall'Amico, M., Zampedri, G., and Rigon, R.: Inventory, distribution and topographic features of rock glaciers in the southern region of the Eastern Italian Alps (Trentino). Geografia Fisica e Dinamica Quaternaria 35, 185–197, doi:10.4461/GFDQ.2012.35.17, 2012.

Shenk, T.: Digital Photogrammetry Vol. 1, Terra Science, Laurelville, OH, USA, 1, 43135, 428 pp., 1999.

Solbø, S. and Storvold, R.: Mapping svalbard glaciers with the cryowing uas, ISPRS-International Archives of the Photogrammetry, Remote Sensing and Spatial Information Sciences, XL-1/W2, 373–377, 2013.

Stumpf, A., Malet, J. P., Allemand, P., Pierrot-Deseilligny, M., and Skupinski, G.: Ground-based multi-view photogrammetry for the monitoring of landslide deformation and erosion, Geomorphology, 231, 130–145, 2015.

Tarolli, P.: High-resolution topography for understanding Earth surface processes: opportunities and challenges, Geomorphology, 216, 295–312, 2014.

Analysis of glacial and periglacial processes using SfM

L. Piermattei et al.

Title Page

Abstract	Introduction
Conclusions	References
Tables	Figures

Back | Close

Full Screen / Esc

Printer-friendly Version

Interactive Discussion

Tonkin, T. N., Midgley, N. G., Graham, D. J., and Labadz, J. C.: The potential of small unmanned aircraft systems and structure-from-motion for topographic surveys: a test of emerging integrated approaches at Cwm Idwal, North Wales, Geomorphology, 226, 35–43, 2014.

Tseng, C.-M., Lin, C. W., Dalla Fontana, G., Tarolli, P.: The topographic signature of a Major Typhoon, Earth Surf. Proc. Land., 40, 1129–1136, 2015.

Verhoeven, G., Karel, W., Štuhec, S., Doneus, M., Trinks, I., and Pfeifer, N.: Mind your grey tones – examining the influence of decolourization methods on interest point extraction and matching for architectural image-based modelling, in: 3D-Arch 2015–3D Virtual Reconstruction and Visualization of Complex Architectures (ISPRS WG V/4, CIPA), 25–27 February 2015, Vol. 40, ISPRS, Avila, Spain, 307–314, 2015.

Wackrow, R. and Chandler, J.: Minimising systematic error surfaces in digital elevation models using oblique convergent imagery, Photogramm. Rec., 26, 16–31, 2011.

Welch, R., and Howarth, P. J.: Photogrammetric measurements of glacial landforms, Photogramm. Rec., 6, 75–96, doi:10.1111/j.1477-9730.1968.tb00915.x, 1968.

Wenzel, K., Rothermel, M., Fritsch, D., and Haala, N.: Image acquisition and model selection for multi-view stereo, Int. Arch. Photogramm. Remote Sens. Spatial Inf. Sci, 251–258, 2013.

Whitehead, K., Moorman, B. J., and Hugenholtz, C. H.: Brief Communication: Low-cost, on-demand aerial photogrammetry for glaciological measurement, The Cryosphere, 7, 1879–1884, doi:10.5194/tc-7-1879-2013, 2013.

Whitehead, K., Moorman, B., and Wainstein, P.: Instruments and Methods Measuring daily surface elevation and velocity variations across a polythermal arctic glacier using ground-based photogrammetry, J. Glaciol., 60, 1208–1220, doi:10.3189/2014JoG14J080, 2014.

Title Page

Abstract | Introduction

Conclusions | References

Tables | Figures

|◀ | ▶|

◀ | ▶

Back | Close

Full Screen / Esc

Printer-friendly Version

Interactive Discussion

Table 1. Date and main parameters of available lidar data.

Date	Aircraft	Laser scanner model	Laser scanner rate	Max. scan angle	Scan frequency	Point density [pts $\cdot$ m^{-2}]
24 Sep 2014	Elicopter AS350 B3	Optech ALTM GEMINI (04SEN164)	100 kHz	46°	34 Hz	5.1
22 Sep 2013	Cessna 404 D-IDOS	ALTM 3100	70 000 Hz	±25°	32 Hz	0.9
17 Sep 2003	–	–	–	–	–	0.5

Table 2. Data acquisition settings and processing results of the photogrammetric surveys for both case studies. The GCPs error is the average transformation residuals error [m] and root mean square reprojection error for the GCPs [pix] during the bundle adjustment computation. The image quality represents the downsized of the images resolution during the dense matching computation. "Ultra high" means full resolution, "High" a downsized of 50 % before the image matching processing. The ground sample distance (GSD) is the average pixel size on the ground. The standard deviation of ICP registration is reported in the table.

	La Mare glacier 4 Sep 2013	27 Sep 2014	Rock glacier 27 Sep 2014
Input data			
Camera type	Nikon 600D	Nikon 600D	Canon 5D Mark III
Focal Length	25 mm	35 mm	28 mm
Image size	5184 × 3456 pix	5184 × 3456 pix	5760 × 3840 pix
N° Images	37	177	198
Processing data			
Reprojection error	0.43 pix (1.76 max)	0.40 pix (3.75 max)	0.38 pix (1.20 max)
GCPs error	1.52 m 1.48 pix	1.14 m 1.96 pix	0.62 m 1.86 pix
Image quality	Ultra high	High	High
Mean GSD	$0.16\,\mathrm{m\,pix^{-1}}$	$0.22\,\mathrm{m\,pix^{-1}}$	$0.064\,\mathrm{m\,pix^{-1}}$
Dense point cloud	49 844 094 pts	55 114 074 pts	56 171 705 pts
Point density	$37\,\mathrm{pts\,m^{-2}}$	$20\,\mathrm{pts\,m^{-2}}$	$244\,\mathrm{pts\,m^{-2}}$
Post-processing data			
Filtered point cloud/subsampled	15 617 342 pts (sampled 0.20 m)	24 226 221 pts (sampled 0.20 m)	4 517 143 pts (sampled 0.10 m)
Point density	$8\,\mathrm{pts\,m^{-2}}$	$9\,\mathrm{pts\,m^{-2}}$	$21\,\mathrm{pts\,m^{-2}}$
ICP transformation	0.14 m	0.15 m	0.10 m

Table 3. Results of comparisons between SfM-MVS-based DTMs vs. ALS-based DTMs in the common area and for the bare-ground stable area and glacier.

DTMs			Elevation differences [m] cell size 1 m × 1 m							
			Common SfM-MVS bare-ground area				Common SfM-MVS glacier area			
			Min	Max	Mean	σ	Min	Max	Mean	σ
SfM-MVS 2013	–	ALS 2013	−19.59	33.61	−0.42	1.72	−9.91	12.04	−0.13	0.78
SfM-MVS 2014	–	ALS 2014	−18.48	22.42	0.03	0.74	−18.17	11.41	0.23	0.65
SfM-MVS 2014	–	SfM-MVS 2013	−33.12	14.19	0.38	1.73	−12.44	12.33	1.58	1.42
ALS 2014	–	ALS 2013	−15.38	10.81	−0.09	0.29	−14.61	7.37	1.30	0.97

Table 4. Mass balance calculations on La Mare Glaciers using different combinations of SfM-MVS and ALS DTMs.

Mass balance estimation								
DTMs cell size 10 m			Spatial coverage [m^2]	Average elevation changes [m]		Volume change [m^3]		Mass balance [m w.e.]
				Raw	Corrected	Raw	Corrected	Raw	Corrected
SfM-MVS 2014	–	SfM-MVS 2013	1 834 800 (∼ 88 %)	1.81	1.45	3 320 988	2 660 460	1.09	0.87
ALS 2014	–	ALS 2013		1.47	1.56	2 697 156	2 862 288	0.88	0.94
SfM-MVS 2014	–	ALS 2013	1 938 700 (∼ 93 %)	1.64	1.70	3 179 468	3 295 790	0.98	1.02
ALS 2014	–	ALS 2013		1.41	1.50	2 733 567	2 908 050	0.85	0.90
ALS 2014	–	ALS 2013	2 072 700 (entire glacier)	1.43	1.52	2 963 961	3 150 504	0.86	0.91

Table 5. Statistics of elevation changes in the rock glacier and in bed ground stable are off rock glacier from Sep 2014 to Sep 2013 and Sep 2003 in the ALS reconstructed area and in the common ALS and SfM-MVS coverage area.

Elevation changes [m]								
	ALS Reconstructed area				SfM-MVS Reconstructed area			
Data	Stable area		Rock glacier		Stable area		Rock glacier	
	Mean	σ	Mean	σ	Mean	σ	Mean	σ
SfM-MVS 2014 – ALS 2014	–	–	–	–	0.05	0.31	0.02	0.17
SfM-MVS 2014 – ALS 2013	–	–	–	–	0.01	0.33	−0.04	0.18
ALS 2014 – ALS 2013	−0.05	0.19	−0.07	0.12	−0.05	0.20	−0.07	0.12
SfM-MVS 2014 – ALS 2003	–	–	–	–	0.06	0.33	−0.16	0.49
ALS 2014 – ALS 2003	−0.01	0.22	−0.18	0.46	−0.00	0.21	−0.18	0.47
ALS 2013 – ALS 2003	0.04	0.21	−0.11	0.41	–	–	–	–

L. Piermattei et al.

Table 6. Velocity statistics in three distinct areas of the rock glacier and in stable area outside the rock glacier evaluated comparing the 2003 and 2014 ALS DTMs and the photogrammetric DTM for the 2014 survey epoch.

| | Horizontal movements between 2003 and 2014 [$cm\,yr^{-1}$] | | | | | | | | |
| | ALS 2003 – ALS 2014 | | | | ALS 2003 – SfM-MVS 2014 | | | | |
	N points	Min	Max	Mean	σ	N points	Min	Max	Mean	σ
Area 1	41	7.3	43.3	26.8	8.9	36	6.8	47.5	26.3	10.3
Area 2	13	4.4	27.4	18.9	7.0	11	9.0	27.9	18.1	6.4
Area 3	26	4.5	16.5	9.4	4.0	24	4.5	18.2	9.0	4.1
Off rock glacier	65	0.0	10.7	3.6	3.1	23	0.0	13.6	5.3	4.2
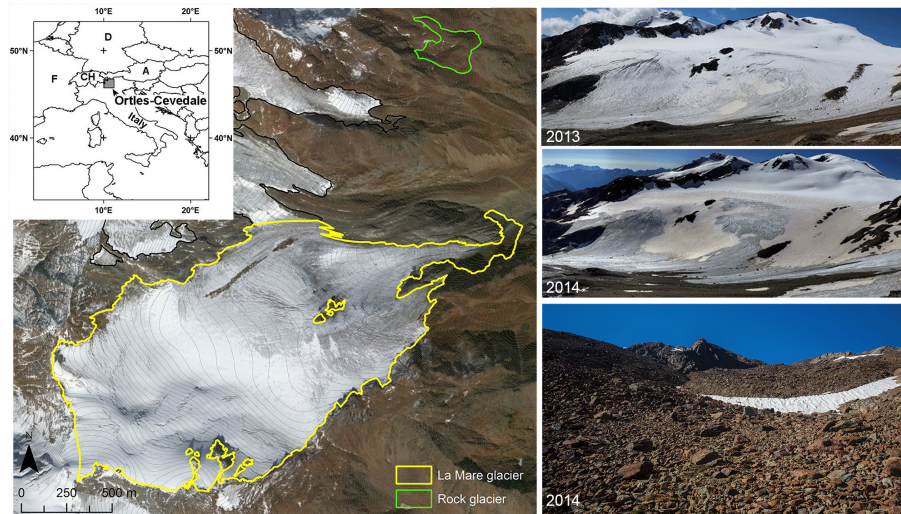
Figure 1. Geographic setting of study areas. Panorama view of the La Mare Glacier from the same camera position on 4 September 2013 and 27 September 2014. The lower right photograph shows the front of the meridional lobe of the AVDM3 Rock Glacier, which was surveyed on 27 September 2014.

● Ground Control Points   ▭ La Mare glacier   ▭ Rock glacier   ▭ Snow 2014   ▨ Active areas off rock glacier
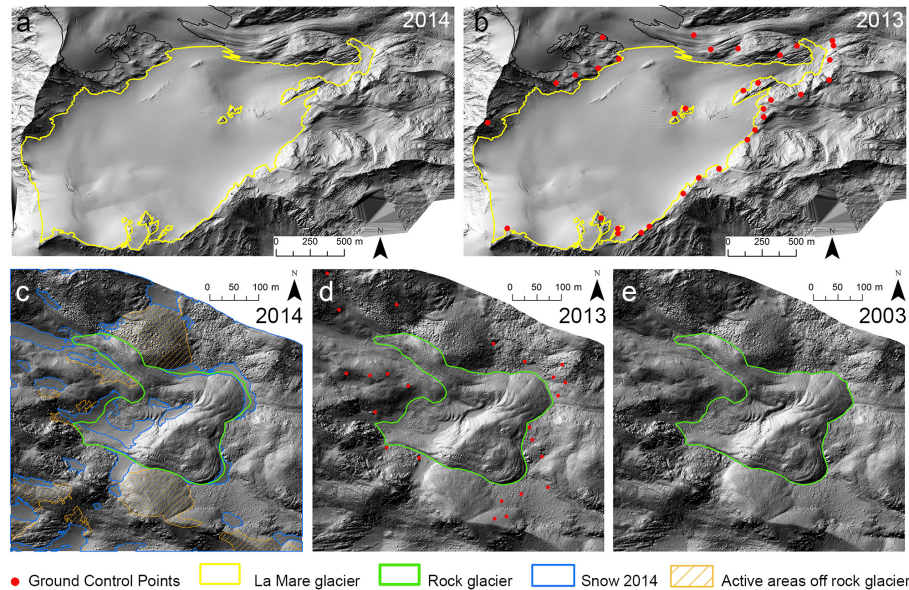
Figure 2. ALS shade DTMs of la Mare glacier acquired on **(a)** 24 September 2014 and **(b)** 21 September 2013. The ALS DTMs of rock glacier acquired on **(c)** 2014, **(d)** 2013 and **(e)** 2003. The red dots represent the selected GCPs in 2013 DTM used in the photogrammetric approach. The snow accumulation areas and geomorphologically-active areas outside the rock glacier were excluded during the ICP computation between 2013 and 2003, 2014 ALS point cloud.
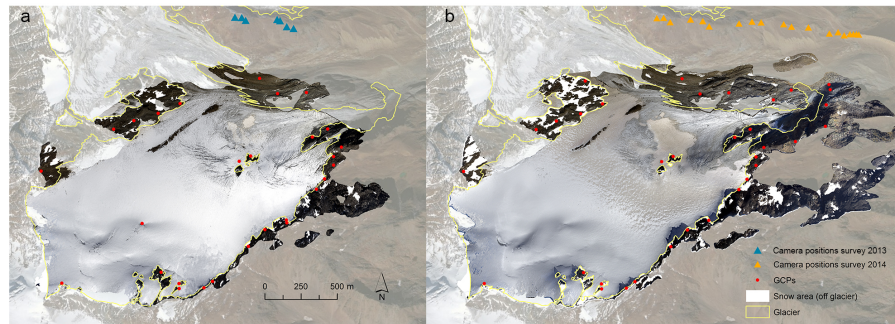
Figure 3. Orthophoto-images of SfM-MVS 3-D model of La Mare glacier surveyed on **(a)** 4 September 2013 and **(b)** 27 September 2014. The white areas in the ortho-images represent the snow-covered area in the rock stable area. The red dots outside the glacier area are the GCPs and the triangles identified the camera locations.

Full Screen / Esc

Printer-friendly Version

Interactive Discussion
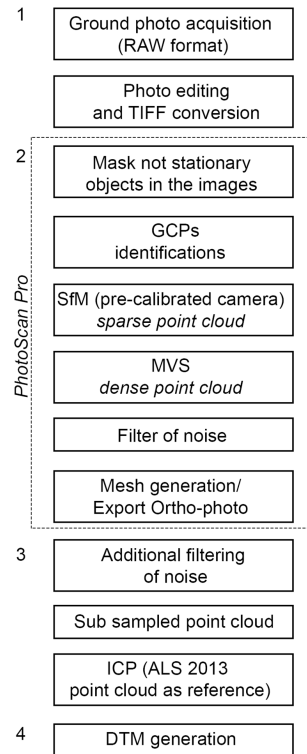
Figure 4. Workflow illustrating the photo-based 3-D reconstruction process used in this work for both case studies, starting from images collection to DTM generation.
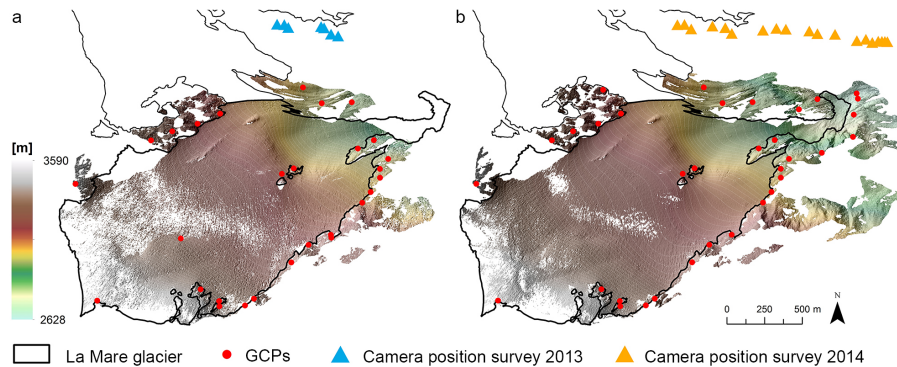
Figure 5. Hillshaded DTMs of La Mare glacier derived from photogrammetric measurements on **(a)** 4 September 2013 and **(b)** 27 September 2014.
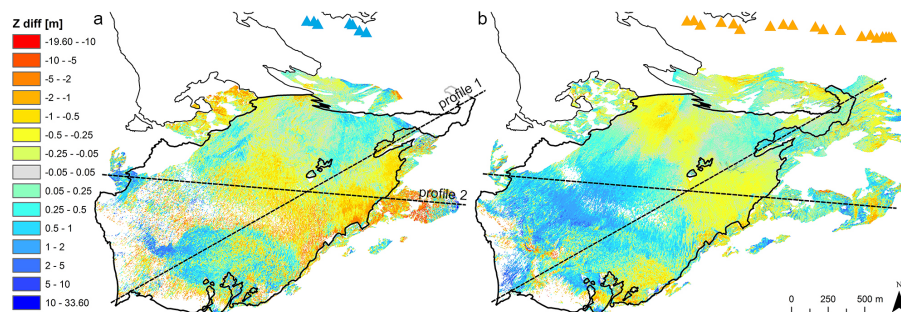
Figure 6. Spatial distribution of elevation differences between photogrammetric and ALS-based DTMs on **(a)** 2013 and **(b)** 2014.
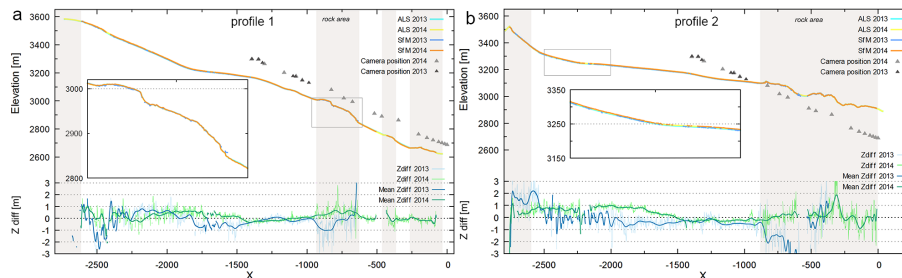
Figure 7. Cross sections through the La Mare glacier DTMs show the glacier elevation change and the difference between 2013 and 2014 in SfM-MVS and ALS-based DTMs. The location of **(a)** the profile 1 and **(b)** profile 2 is indicated in Fig. 6. The *x* axis zero has been fixed at the first camera position of the 2014 survey and the minimum and maximum values of the *z*-difference set to ±3 m.
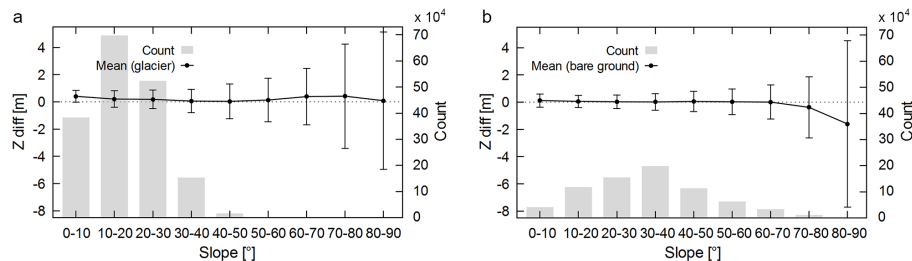
Figure 8. Mean and standard deviation of the 2014 DoD between SfM-MVS and ALS-based DTM depending on slope calculated **(a)** in the glacier area and **(b)** in the bare ground outside glacier covered by rock. The grey bars show the count of cells at any given slope (*y* axis on the right).
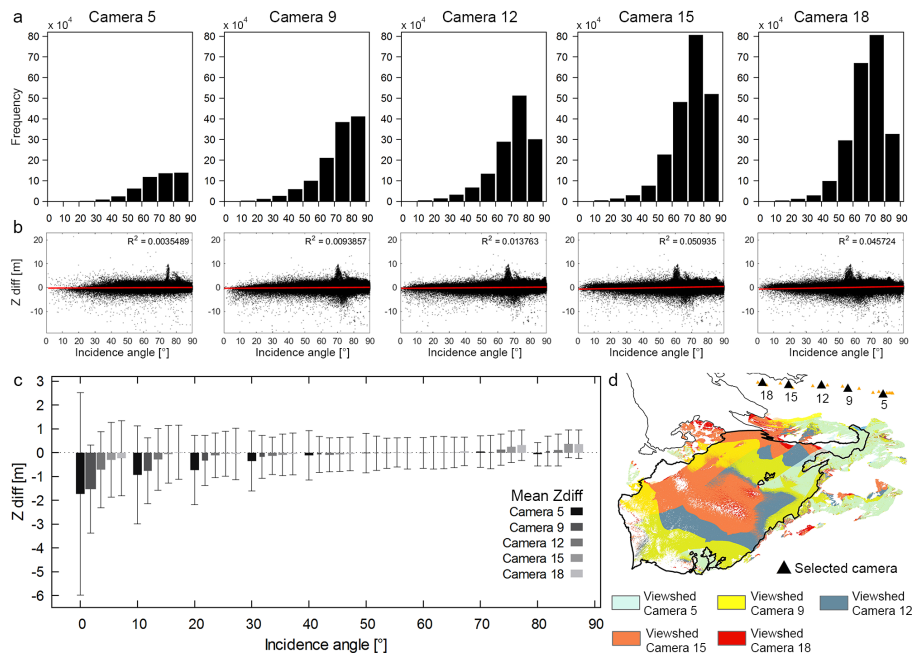
Figure 9. Incidence angles between five cameras positions and vectors normal to the surface. **(a)** Frequency distribution histograms of incidence angles calculated for the corresponding surface and **(b)** the scatterplot of the elevation difference and incidence angle for the five camera positions; **(c)** mean of elevation differences with one standard deviation y bars calculated for each camera and for incidence angle intervals; **(d)** map of the locations of the selected cameras with the viewshed reconstructed area visible from each camera point.
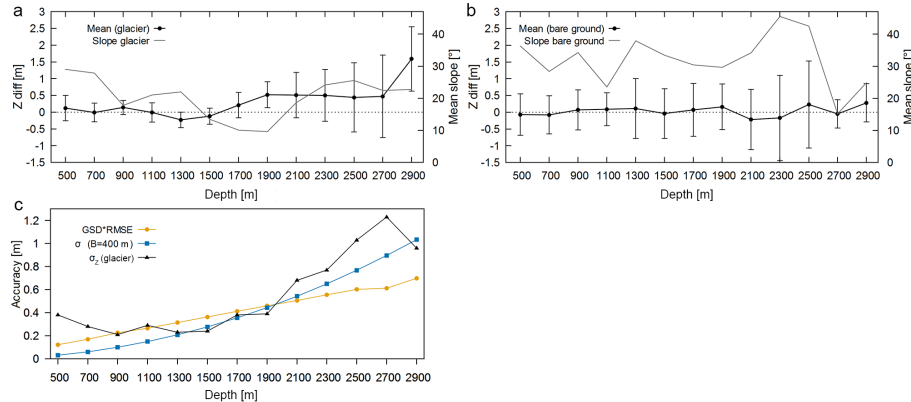
Figure 10. Mean and standard deviation of the 2014 DoD between SfM-MVS and ALS-based DTM depending on depth calculated **(a)** in the glacier area and **(b)** in the bare ground outside glacier covered by rock. The trend of the average slope angle for depth intervals is shown on the right y axis. **(c)** Comparison of σ_z measured in the glacier reconstructed area, the theoretical depth accuracy estimated according to the Eq. (1) and the GSD multiplied for the GCPs RMSE for the depth intervals.
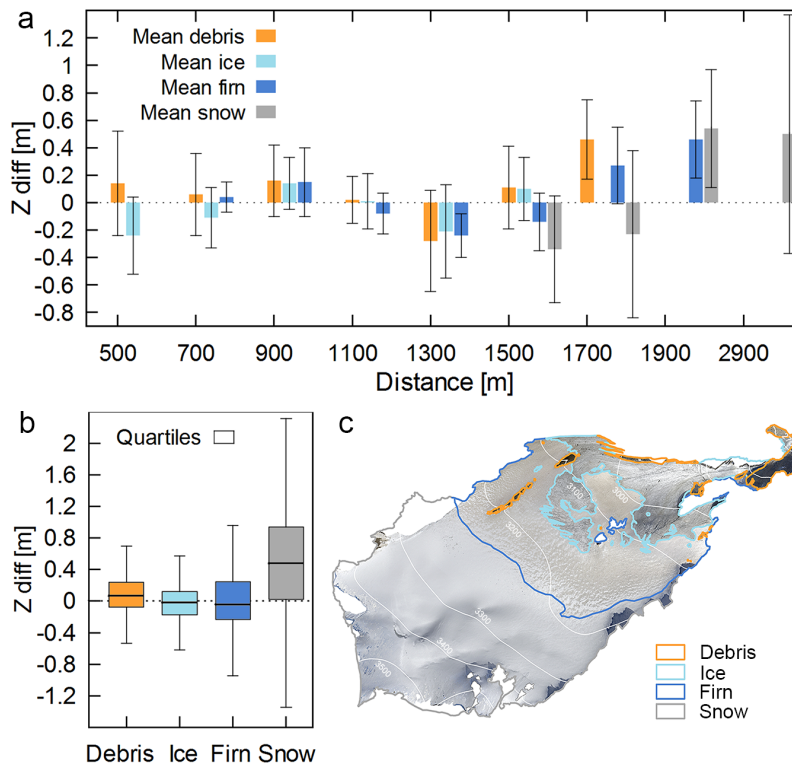
Figure 11. Elevation difference between the 2014 SfM-MVS and ALS-based DTMs calculated for different substrata. The figure shows **(a)** the mean and standard deviation of *z*-difference for four substrata (debris, ice, firn, and snow) grouped by distance from camera position; **(b)** the box plot of the *z*-difference for four substrata. In the box-whisker plot, values which exceed 1.5× IQR were considered outliers. In panel **(c)** the orthophoto of the glacier on 27 September 2014 and map of substrata.

ESURFD

3, 1345–1398, 2015

Analysis of glacial and periglacial processes using SfM

L. Piermattei et al.

Title Page

Abstract	Introduction
Conclusions	References
Tables	Figures

◄	►
◄	►

| Back | Close |

| Full Screen / Esc |

Printer-friendly Version

Interactive Discussion
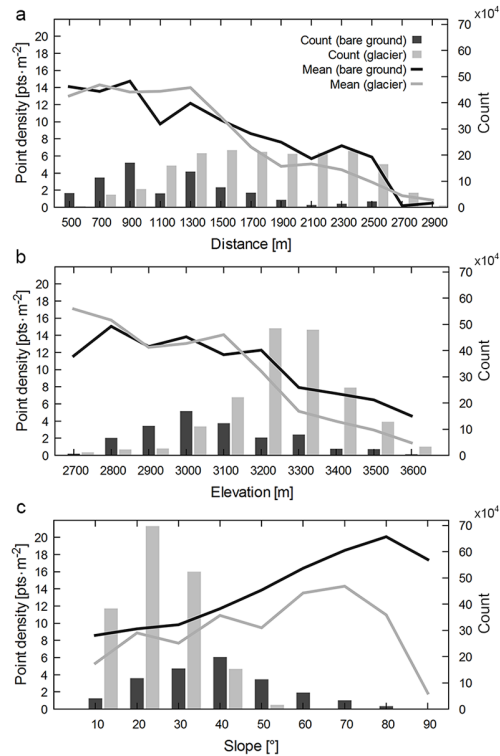
Figure 12. Relationships between point density of the 2014 photogrammetric 3-D model and **(a)** camera–object distance, **(b)** elevation and **(c)** slope calculated for the glacier and rock stable area outside glacier. The point density was estimated using the filtered and subsampled point cloud.
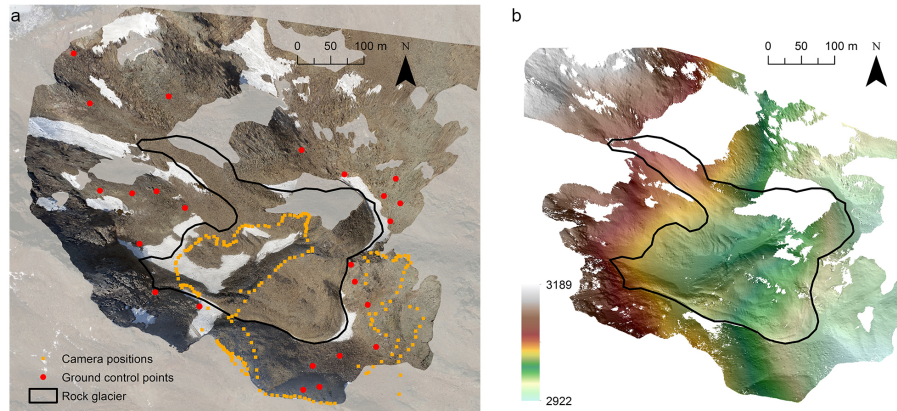
Figure 13. Correspondence between **(a)** the orthophoto of SfM-MVS 3-D model of rock glacier surveyed on 27 September 2014 and **(b)** the hillshade model of rock glacier model calculated at the same data and hour of the images acquisition. The holes in the DTM represent not reconstructed area.
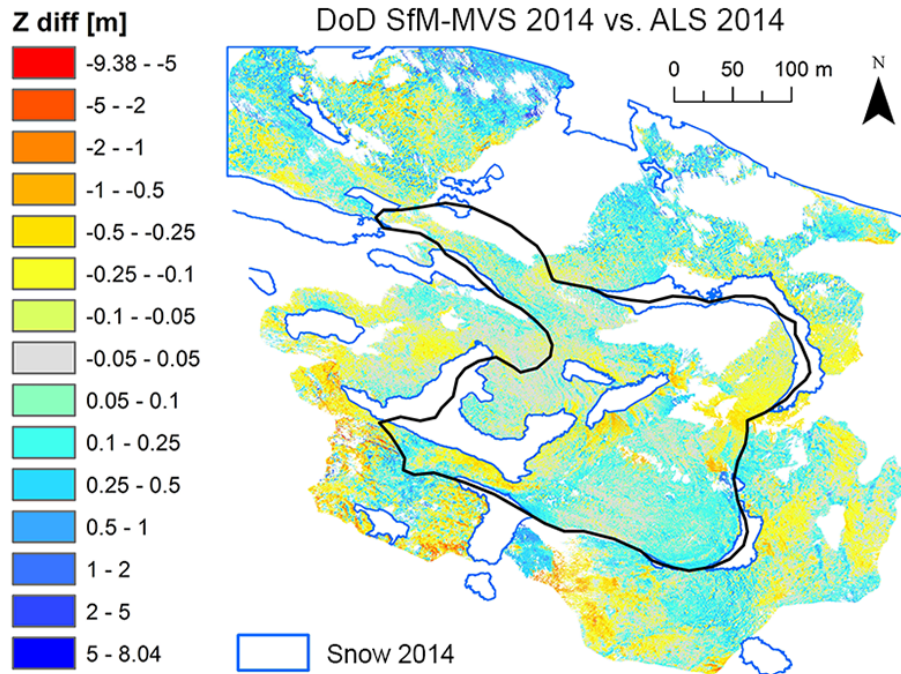
Figure 14. Spatial distribution of elevation differences between photogrammetric and ALS-based DTM acquired on 27 September 2014 and 24 September 2014, respectively. The blue shape is the snow accumulation areas excluded during the DTMs comparison.

Full Screen / Esc

Printer-friendly Version

Interactive Discussion

Figure 15. Elevation differences between 2014 SfM-MVS and ALS-based DTMs calculated for the slope interval **(a)** in the rock glacier reconstructed area and **(b)** in the bare ground outside the rock glacier.

Figure 16. Elevation differences between 2014 SfM-MVS and ALS-based DTMs calculated for the hillshade interval **(a)** in the rock glacier reconstructed area and **(b)** in the bare ground outside the rock glacier. Lowest values represent shadowed area whilst lighted areas present the highest values.
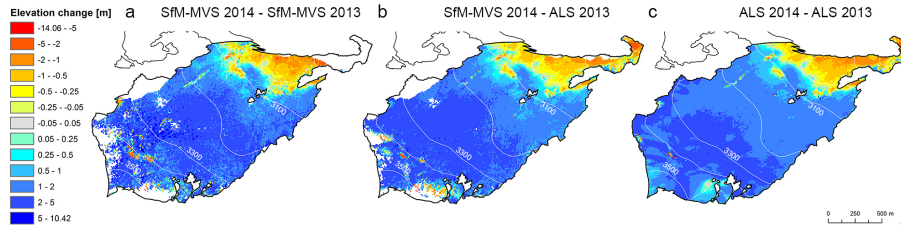
Figure 17. Spatial distribution of elevation changes between **(a)** SfM-MVS 2014 and SfM-MVS 2013 DTMs **(b)** SfM-MVS 2014 and ALS 2013 over the area of the glacier with common coverage and **(c)** ALS 2014 and ALS 2013 over the entire glacier.
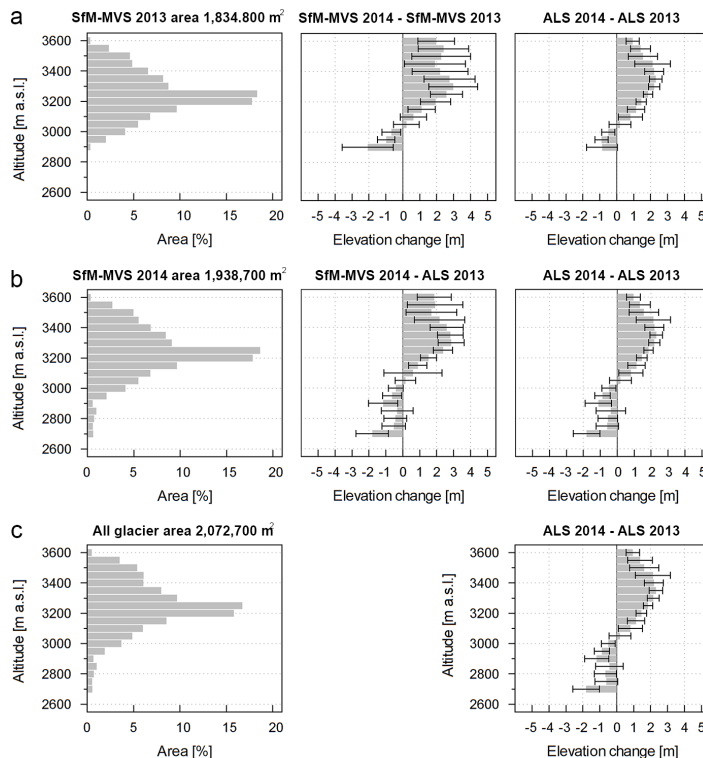
Figure 18. Area-altitude distribution and surface elevation change with standard deviation for the glaciological year 2014/13 displayed for altitudinal bands with 50 m interval. The elevation change were calculated between **(a)** SfM-MVS DTMs of 2013 and 2014 in the 2013 photogrammetric reconstructed area; **(b)** SfM-MVS DTMs of 2014 and ALS DTM of 2014 in the 2014 photogrammetric reconstructed area; **(c)** ALS DTMs of 2013 and 2014 of the entire glacier. The photogrammetric results were compared with the corresponding ALS result calculated in the same area.
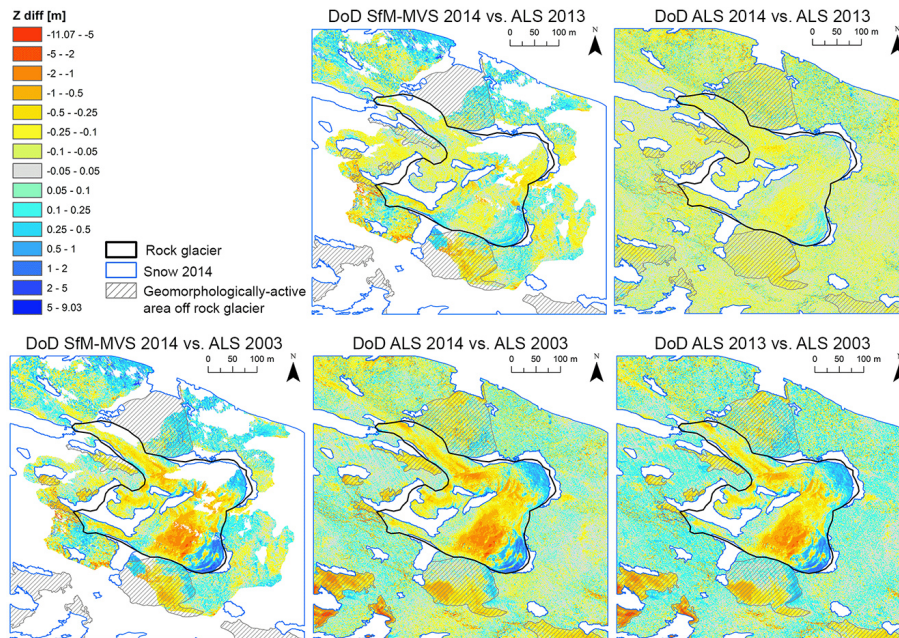
Figure 19. Spatial distribution of elevation changes from September 2014 to September 2013 and September 2003 between the DTMs derived from SfM-MVS and ALS.
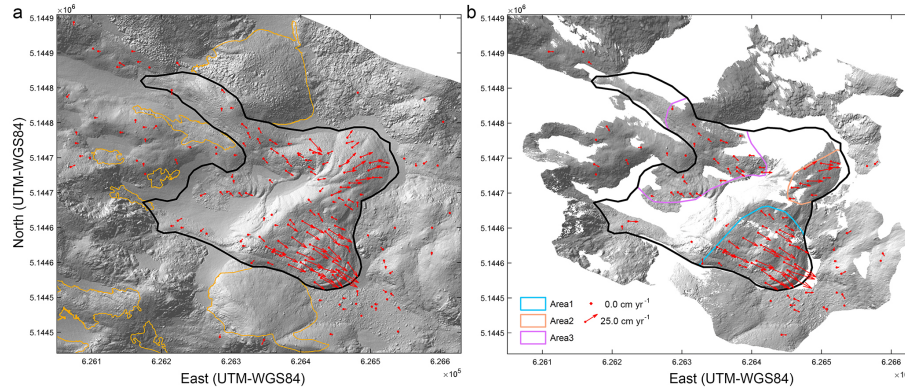
Figure 20. Displacement vectors of the rock glacier between 2003 and 2014 computed by a manual identification of natural features visible in the shaded DTMs generated by **(a)** ALS for both survey epochs and by **(b)** ALS and photogrammetry for 2003 and 2014 survey, respectively.